Rev. Adv. Mater. Sci. 41 (2015) 20-34

STRESS-DRIVEN ROTATIONS OF DEFORMATION-DISTORTED GRAIN BOUNDARIES IN NANOCRYSTALLINE AND ULTRAFINE-GRAINED MATERIALS

S.V. Bobylev[1,2,3] and I.A. Ovid'ko[1,2,3]

[1]Department of Mathematics and Mechanics, St. Petersburg State University, St. Petersburg 198504, Russia
[2]Institute of Problems of Mechanical Engineering, Russian Academy of Sciences, Bolshoj 61, Vasilievskii Ostrov, St. Petersburg 199178, Russia
[3]St. Petersburg State Polytechnical University, St. Petersburg 195251, Russia

Received: May 3, 2014

Abstract. A special mechanism/mode of plastic deformation occurring through stress-driven rotations of deformation-distorted grain boundaries (GBs) in nanowires, micropillars, thin films and subsurface areas of bulk solids with nanocrystalline and ultrafine-grained structures is theoretically described. The suggested approach serves as a generalization of the theoretical model [Bobylev and Ovid'ko, Phys. Rev. Lett. 109, 175501 (2012)] describing stress-driven rotations of regular (non-distorted) low-angle tilt boundaries composed of periodically arranged lattice dislocations in crystals. In the exemplary case of nickel specimens with nanocrystalline and ultrafine-grained structures, it is found that the rotations of deformation-distorted GBs are energetically favorable processes in wide range of GB parameters. Each energetically favorable GB rotation is specified by its equilibrium rotation angle φ_{eq} associated with the energy minimum. Dependences of φ_{eq} on applied stress, GB misorientation and other geometric characteristics of a rotating GB are calculated which show the trends in realization of stress-driven rotations of deformation-distorted GBs in nanocrystalline and ultrafine-grained solids. Also, combined splitting and rotations of deformation-distorted GBs are theoretically described as energetically favorable processes in wide ranges of parameters characterizing GB configuration. These processes result in formation of nanoscale grains in nanocrystalline and ultrafine-grained solids. Our theory is consistent with the corresponding experimental data reported in the literature.

1. INTRODUCTION

Plastic deformation and fracture processes occurring in nanowires, micropillars, nanocrystalline and ultrafine-grained (UFG) solids represents the subject of intensive research efforts in materials science and physics of nanostructured solids; see, e.g., [1-27]. In particular, specific (inherent to nanostructures) physical mechanisms of plastic flow are of utmost interest which effectively operate in nanocrystalline and UFG bulk solids due to the combined *nanoscale and grain-boundary effects* (Fig. 1a) [1–3,6,7,10–15,18,21-24,26]. In nanowires and micropillars typically having single crystalline structures, the combined *nanoscale and free-surface effects* strongly influence plastic deformation processes (Fig. 1b). In particular, with these effects, both lattice dislocation starvation [5] and specific mechanisms of plastic flow come into play in single crystalline nanowires and micropillars [5,8,9,12,16,20,27]. Recently, a particular attention has been paid to nanowires, micropillars and thin films with nanocrystalline and UFG structures as

Corresponding author: I.A. Ovidko, e-mail: ovidko@nano.ipme.ru

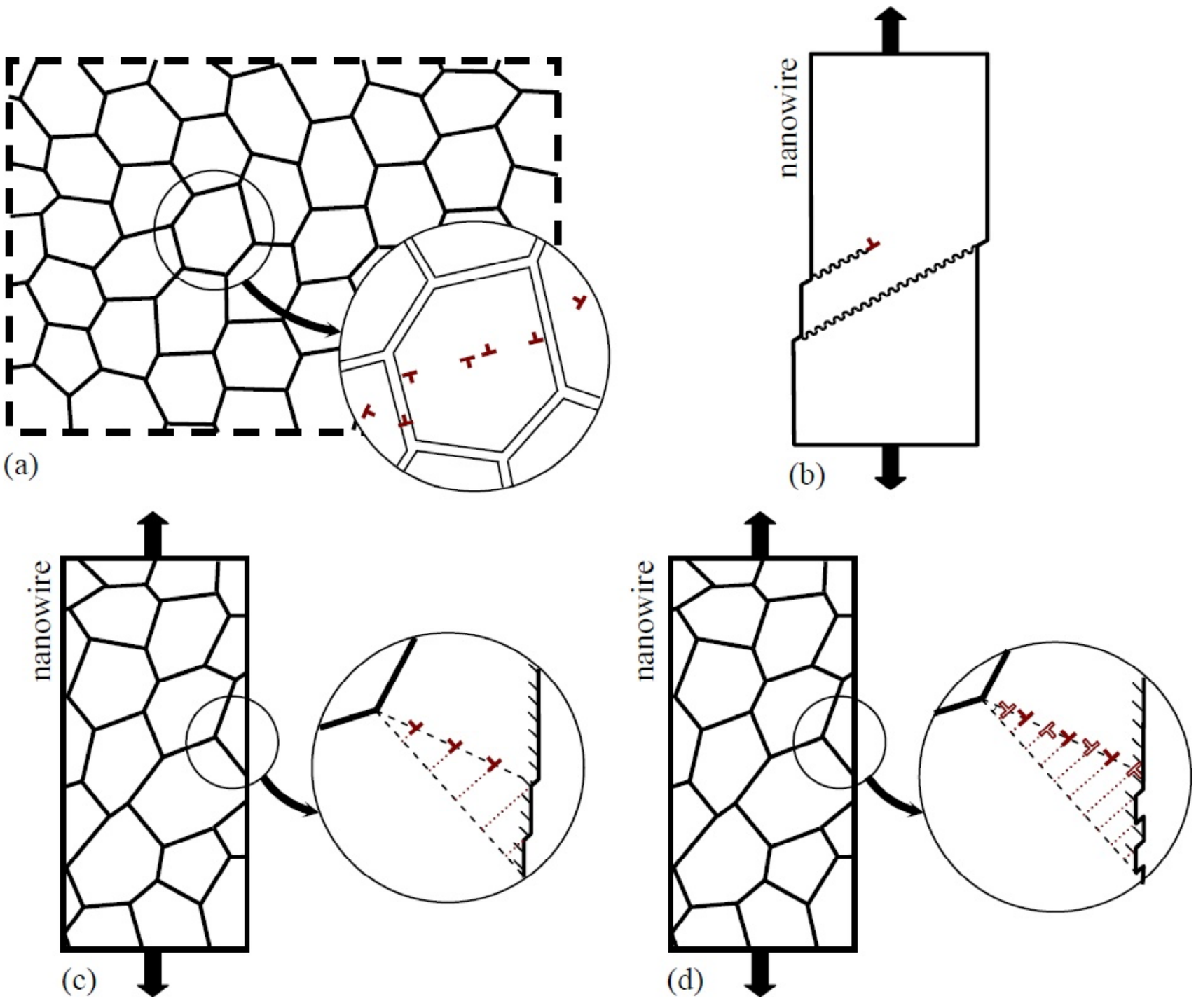

Fig. 1. (Color online) Structural and geometric effects on physical mechanisms of plastic deformation occurring in various solids. (a) Nanocrystalline/ultrafine-grained bulk solid is schematically shown where the combined *nanoscale and grain-boundary effects* effectively operate influencing physics of plastic deformation processes. In particular, as it is illustrated in a magnified inset, nanoscale dislocation slip controlled by dislocation emission from grain boundaries and dislocation absorption at grain boundaries significantly contributes to plastic flow. (b) Single crystalline nanowire is schematically shown where the combined *nanoscale and free-surface effects* effectively operate influencing physics of plastic deformation processes. In particular, nanodisturbances (nanoscale areas where ideal plastic shear occurs) generated at free surfaces can contribute to plastic flow in nanowires. (c) Nanocrystalline/ultrafine-grained nanowire is schematically shown where the combined *nanoscale, grain-boundary and free-surface effects* effectively operate. In particular, as it is illustrated in a magnified inset, stress-driven rotations of non-distorted grain boundaries can contribute to plastic flow. (d) Nanocrystalline/ultrafine-grained nanowire containing deformation-distorted grain boundaries is schematically shown where the combined *nanoscale, grain-boundary, deformation-distorted-GB-structure and free-surface effects* effectively operate influencing physics of plastic deformation. In particular, as it is illustrated in a magnified inset, stress-driven rotations of deformation-distorted grain boundaries can contribute to plastic flow.

solids where the three effects - the *nanoscale, grain-boundary, and free-surface effects* - cooperatively operate which can cause actions of unusual mechanisms of plastic deformation (Fig. 1c) [25,28–32]. For instance, the experiment [30] revealed GB transformations of a new type – GB rotations – to occur in nanocrystalline Ni nanopillars under mechanical load. In Letter [33], GB rotations were theoretically described as stress-driven processes representing a new physical mechanism of plastic deformation in solids (Fig. 1c). As it has been demonstrated in Letter [33], stress-driven rotations of low-angle GBs with regular dislocation structures effectively carry plastic flow and transform GB defect configurations in nanocrystalline nanowires, nanopillars and films as well as subsurface areas of bulk nanocrystalline solids due to the combined actions of the nanoscale, grain-boundary and free-surface effects.

In Letter [33], we theoretically described stress-driven rotations of low-angle tilt boundaries with regular structures – GBs of the simplest geometric type - modeled as finite walls of periodically arranged

lattice dislocations. Along with such simplest GBs, deformation-distorted GBs are often present in nanocrystalline and UFG solids. First of all, deformation-distorted GBs are intensively formed in nanocrystalline and UFG metals fabricated by severe plastic deformation methods [34-36]. Such GBs contain high densities of extrinsic dislocations and other defects, in which case solids with deformation-distorted GBs exhibit unusual mechanical and physical properties. For instance, deformation-distorted GBs in UFG metals are viewed to be responsible for their superior strength, high diffusivity, good electrical conductivity, as well as optimization of strength and ductility; see reviews [35-37]. As a consequence, the presence of deformation-distorted GBs serves as a well distinguished structural factor capable of causing its specific dramatic effects on the outstanding properties of nanocrystalline and UFG solids. That is, one can add the effects of deformation-distorted GBs to the set of the effects that (i) are originated from the structural and geometric factors; and (ii) strongly influence mechanical and physical properties of solids.

In the context discussed, there is large interest in describing the behavior of solids where the four effects - the *nanoscale, grain-boundary, deformation-distorted-GB-structure, and free-surface effects* - cooperatively operate which can cause actions of unusual physical mechanisms of plastic deformation (Fig. 1d). The main aim of this paper is to examine and theoretically describe a new mechanism of plastic deformation – rotations of deformation-distorted GBs - in nanocrystalline and UFG solids (nanowires, micropillars, thin films and subsurface areas of bulk solids), with the four effects taken into account. In doing so, we will extend the approach [33] to the case of deformation-distorted GBs and theoretically describe their stress-driven rotations carrying plastic deformation in nanocrystalline and UFG solids. In addition, a new phenomenon – formation of nanoscale grains through stress-driven splitting and rotation of deformation-distorted GBs – will be predicted and theoretically examined.

2. STRESS-DRIVEN ROTATIONS OF DEFORMATION-DISTORTED GRAIN BOUNDARIES: GEOMETRIC ASPECTS

Let us consider geometric features of plastic deformation mode occurring through stress-driven rotations of deformation-distorted low-angle tilt boundaries in nanocrystalline and UFG solids (Fig. 2). (For shortness, hereinafter both nanocrystalline and UFG solids - nanowires, micropillars, thin films and bulk solids with nanocrystalline and UFG structures - will be called nanostructured solids). Fig. 2a schematically shows a two-dimensional section of a nanostructured solid consisting of nanoscale/ultrafine grains divided by GBs. The subsurface area of the solid contains a deformation-distorted low-angle tilt boundary AB which is presented in the magnified inset in Fig. 2b. The GB AB plane makes the angle α with the specimen free surface and has the common point B with the free surface (Fig. 2b). Also, the GB AB forms the triple junction A with two static GBs AC and AD (Fig. 2b).

We now consider the structural features of a deformation-distorted low-angle GB near the solid free surface. To do so, we exploit representations of the model [38] describing a typical deformation-distorted low-angle GB as a dislocation wall configuration consisting of both "equilibrium" and "non-equilibrium" perfect dislocations of the edge type (Fig. 3). The equilibrium dislocations (full dislocation signs in Fig. 3) of each dislocation-distorted GB have Burgers vectors $\boldsymbol{b}$ and form a periodic wall specified by period p (Fig. 3). The periodic wall of equilibrium dislocations provides a constant contribution θ to the tilt misorientation of the deformation-distorted GB, where $\theta \approx b/p$.

In general, the tilt misorientation of a deformation-distorted GB fluctuates along the GB, and the non-equilibrium dislocations (open dislocation signs in Fig. 3) are responsible for such fluctuations. Following Ref. [38], we consider the non-equilibrium dislocations of a deformation-distorted GB as edge dislocations having positive and negative Burgers vectors $\mathbf{b}$ and $-\mathbf{b}$, respectively (Fig. 3). For definiteness, we suppose that the non-equilibrium dislocations of the GB form a periodic structure consisting of short dislocation walls with alternate orientations of dislocation Burgers vectors (Fig. 3). That is, the non-equilibrium dislocation ensemble consists of short walls, each containing M dislocations, and dislocations signs within one walls are the same, while dislocation signs in neighboring short walls are different. The total number of non-equilibrium dislocations in the deformation-distorted GB is $2MN_1$, with N_1 being a positive integer. As a corollary, the sum Burgers vector of all the non-equilibrium dislocations of the GB is equal to zero, and the GB tilt misorientation periodically fluctuates around its mean value θ determined by the equilibrium dislocations. Figs. 3a, 3b, and 3c illustrate the three deformation-distorted GB structures specified by M = 1, 2, and 3, respectively.

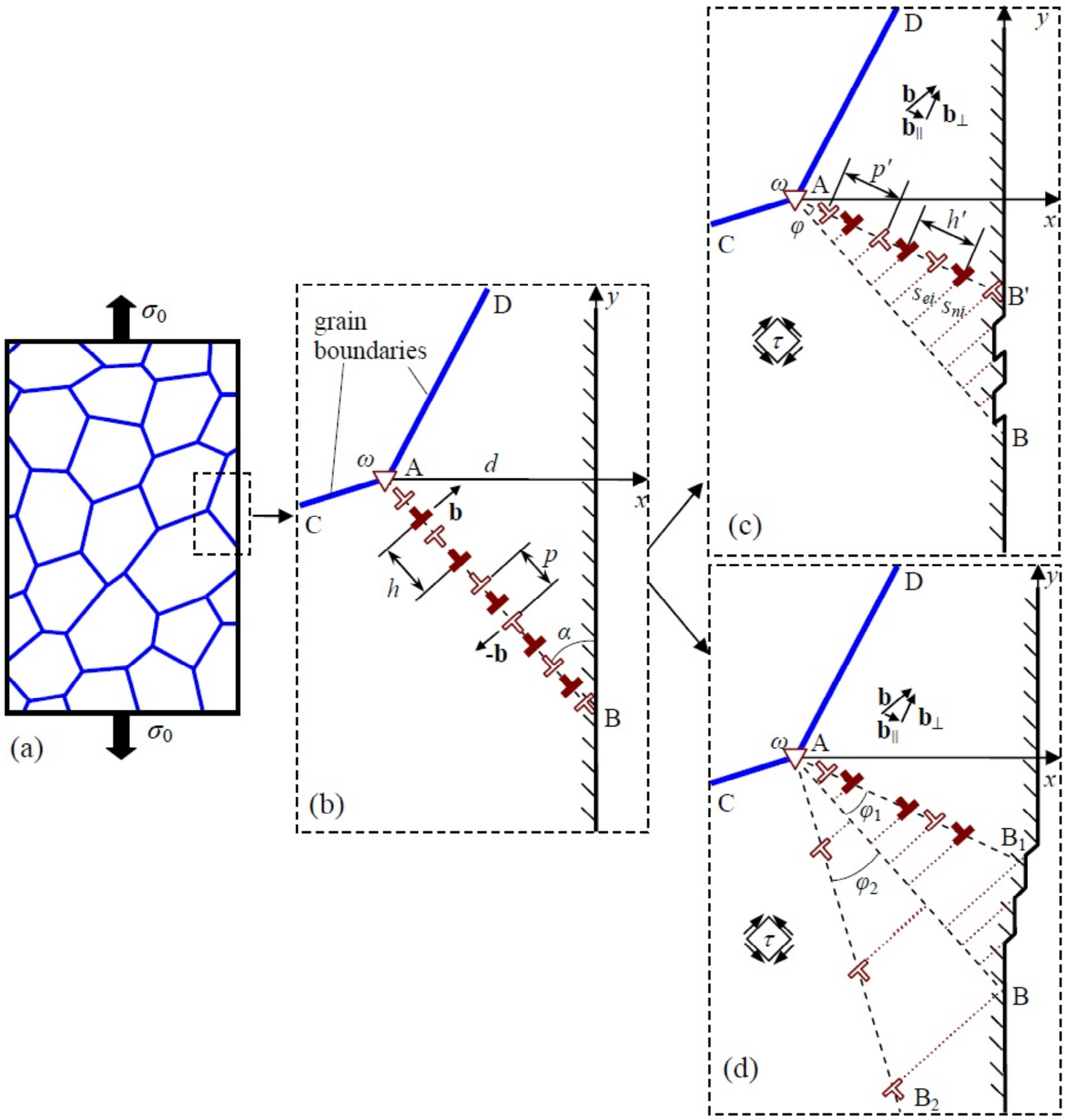

Fig. 2. (Color online) Rotations of deformation-distorted grain boundaries. (a) A nanocrystalline/ultrafine-grained specimen (a general view). (b) Initial state. Following [38], deformation-distorted grain boundary AB is modeled as superposition of two dislocation ensembles: a regular wall of equilibrium dislocations (full dislocation signs) with Burgers vectors **b** and an ensemble of non-equilibrium dislocations (open dislocation signs) having positive and negative Burgers vectors **b** and **–b**. For definiteness, we suppose that the non-equilibrium dislocations of the deformation-distorted grain boundary form a periodic structure consisting of short dislocation walls with alternate orientations of dislocation Burgers vectors. That is, the non-equilibrium dislocation ensemble consists of short walls, each containing *M* dislocations, and dislocations signs within one walls are the same, while dislocation signs in neighboring short walls are different. (c) Cooperative slip of edge dislocations belonging to grain boundary under the shear stress τ leads to grain boundary rotation by angle φ. In doing so, several dislocations enter the free surface where they disappear and generate free surface steps. (d) The shear stress σ causes slip of dislocations with various Burgers vectors in two opposite directions. As a result, the initial grain boundary splits into two grain boundaries, AB_1 and AB_2, that rotate in opposite directions by angles φ_1 and φ_2, respectively.

Let us consider rotation of a deformation-distorted GB AB located near the solid free surface (Fig. 2). Our further analysis is rather general; it is relevant for deformation-distorted GBs with various values of their basic structural parameters *M*, *p,* and *h*. At the same time, for definiteness, Fig. 2 presents the case of the GB characterized by $M = 1$ and $p / h = 1$. In doing so, ensembles of “equilibrium” and “non-equilibrium” dislocations are shifted by $h / 2$ relative each other in order to avoid both annihilation and merging of the “equilibrium” and “non-equilibrium” dislocations.

As it has been noted above, three tilt GBs AB, CA, and DA join to the triple junction A. The tilt

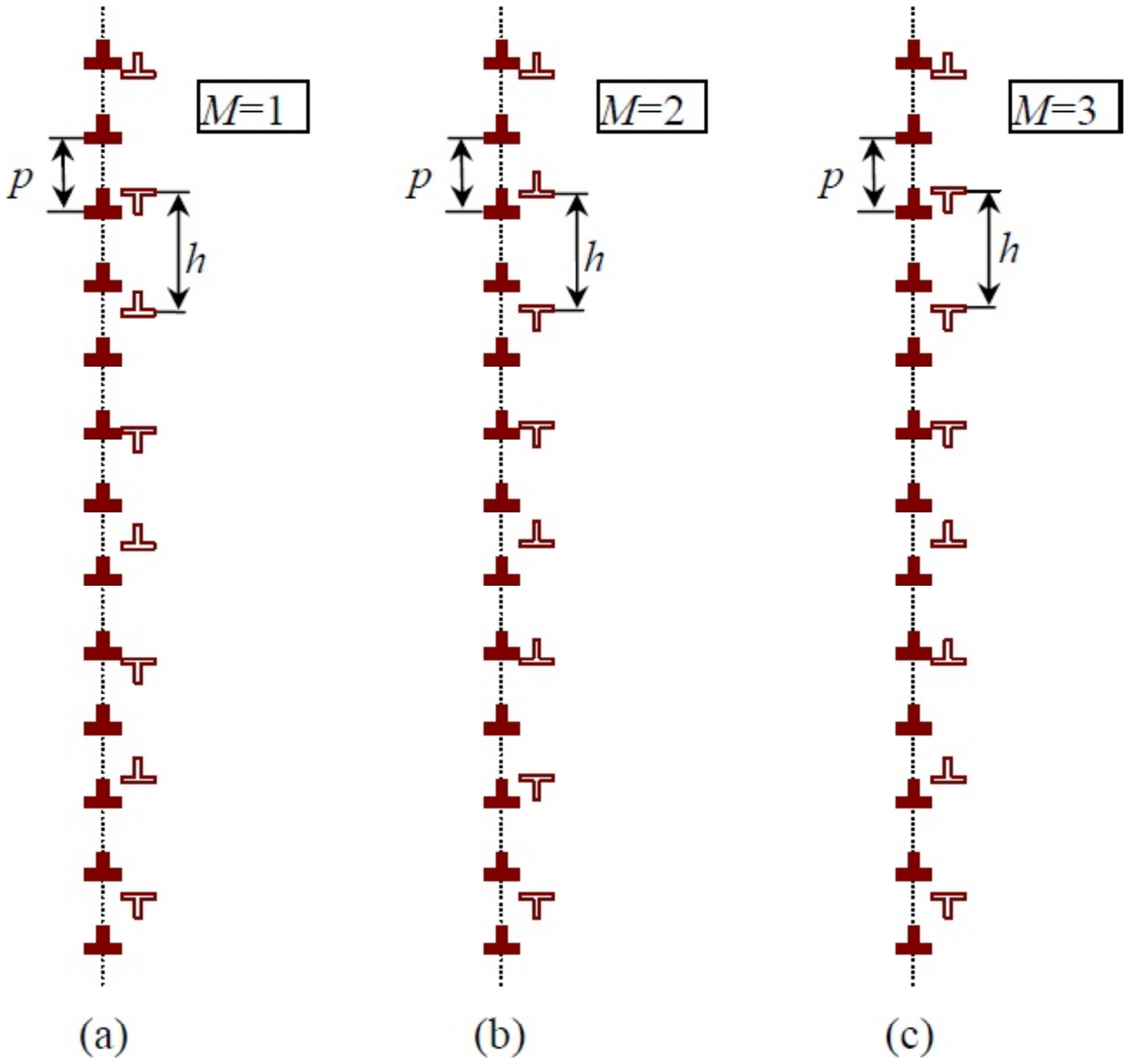

Fig. 3. (Color online) Dislocation structures of deformation-distorted grain boundaries for various values of parameter *M* (for details, see text). (a) *M* = 1; (b) *M* = 2; (c) *M* = 3.

misorientation angles of the GBs AB, CA, and DA at the triple junction A in the initial state of the system (before the GB AB rotation; see Figs. 2a and 2b) are balanced, in which case the triple junction A does not create stresses. We assume that the GBs CA and DA are static, and their structures are unchanged during the GB AB rotation. In this case, following the approach [33], the effect of the two static GBs CA and DA on the GB AB rotation is in their combined role as a disclination stress source at the triple junction A. More precisely, the GBs CA and DA cooperatively serve as the wedge disclination A whose strength ω in the initial state of the system is equal by magnitude and opposite in sign to the tilt misorientation θ of the GB AB: $\omega = -\theta$. The latter equation describes the considered situation where the tilt misorientation angles of the GBs AB, CA and DA at the triple junction A before the GB AB rotation (Figs. 2a and 2b) are balanced, and the triple junction A does not create stresses.

The dislocations of the GB AB under the shear stress τ (acting in the dislocation glide plane) move to their new positions (Fig. 2c). Following the approach [33], during movement of the dislocations, the GB AB composed of these dislocations is flat and thus moves to its new position AB' (Fig. 2c). (The condition that the GB is flat follows from the demand that the energy of the GB should be minimal during movement of the GB dislocations. The above statement is based on our analysis whose space-consuming presentation is beyond the scope of this paper.) That is, in fact, the GB AB (Fig. 2b) rotates over some angle φ around the triple junction A to its new position AB' (Fig. 2c).

During the rotation of the GB, its structural geometry changes. In particular, in the case illustrated in Fig. 2c, a part of the dislocations of the rotating GB disappear at the free surface due to the GB rotation, and the corresponding free surface steps are formed. Also, by analogy with the case of regular low-angle tilt boundaries [33], the deformation-distorted GB AB transforms from symmetric tilt boundary in the initial state (Fig. 2b) into asymmetric one in the final state after the rotation (Fig. 2c). It is related to the fact that the Burgers vectors of GB dislocations change their orientation relative to the GB plane during its rotation. That is, after the rotation of the GB, the Burgers vector of each of its dislocations located at the GB plane AB' has non-zero components parallel and perpendicular to the GB plane AB' (Fig. 2c), in contrast to the initial GB state in which the parallel component is zero (Fig. 2b).

In addition, the tilt misorientation angle of the GB decreases ($\theta \rightarrow \theta'$), where $\theta' < \theta$) due to the GB rotation, because the perpendicular component of Burgers vectors characterizing its dislocations after the GB rotation (Fig. 2c) decreases, as compared to that in the initial GB state (Fig. 2b). The decrease in the tilt misorientation angle violates the balance $\omega = -\theta$ of the misorientation angles of the GBs at the triple junction A, and thereby this junction A becomes a stress source whose elastic energy represents the main hampering force for the GB rotation process.

The key contribution to the driving force for the GB rotation is related to plastic deformation work associated with the stress-driven dislocation glide. In doing so, some of the dislocations enter the free surface where they disappear and create the corresponding steps (Fig. 2c). The step length is equal to the Burgers vector magnitude *b* characterizing the dislocation entering the solid free surface. In next section, we will consider the balance of the driving and hampering forces for the GB rotation (Fig. 2c) and reveal dependences of the characteristic rotation angle on parameters of the system under our study.

Note that, along with stress-driven rotation of the GB AB (Figs. 2b and 2c), the system can evolve through splitting of the initial GB AB into two GBs that rotate in opposite directions (Figs. 2b and 2d). This combined splitting and rotation process (resulting in formation of the nanoscale grain B_1AB_2; see Fig. 2d) will be examined in detail in sections 4 and 5.

3. STRESS-DRIVEN ROTATIONS OF DEFORMATION-DISTORTED GRAIN BOUNDARIES: ENERGY AND EQUILIBRIUM ROTATION ANGLE

Let us calculate the equilibrium angle that characterizes rotation of the GB AB (Fig. 2b) to its new position AB' (Fig. 2c) as a function of various parameters of the system. The equilibrium angle corresponds to the minimum of the energy change ΔW_{rot} related to the GB rotation. The energy change is given as:

$$\Delta W_{rot} = W_1 - W_0 - A, \tag{1}$$

where W_0 and W_1 are the energies of the system in its final and initial states, respectively, and A is the work spent by the shear stress τ on movement of the dislocations belonging to the rotating GB.

In terms of the theory of defects in solids, the energies W_0 and W_1 are written as follows:

$$\begin{aligned} W_0 = {} & W^{\Delta} + \sum_{i=1}^{n} W^{d}(x_{ei}) + \sum_{i=1}^{k} W^{d}(x_{ni}) + \sum_{i=1}^{n} W^{\Delta-d}(d, x_{ei}, y_{ei}) + \sum_{i=1}^{k} W^{\Delta-d}(d, x_{ni}, y_{ni}) + \\ & \sum_{i=1}^{n-1}\sum_{j=i+1}^{n} W^{d-d}(x_{ei}, x_{ej}, y_{ei} - y_{ej}) + \sum_{i=1}^{k-1}\sum_{j=i+1}^{k} W^{d-d}(x_{ni}, x_{nj}, y_{ni} - y_{nj}) + \sum_{i=1}^{n}\sum_{j=1}^{k} W^{d-d}(x_{ei}, x_{nj}, y_{ei} - y_{nj}), \end{aligned} \tag{2}$$

$$\begin{aligned} W_1 = {} & W^{\Delta} + \sum_{i=1}^{n'} W^{d}(x'_{ei}) + \sum_{i=1}^{k'} W^{d}(x'_{ni}) + \sum_{i=1}^{n'} W^{\Delta-d}(d, x'_{ei}, y'_{ei}) + \sum_{i=1}^{k'} W^{\Delta-d}(d, x'_{ni}, y'_{ni}) + \\ & \sum_{i=1}^{n'-1}\sum_{j=i+1}^{n'} W^{d-d}(x'_{ei}, x'_{ej}, y'_{ei} - y'_{ej}) + \sum_{i=1}^{k'-1}\sum_{j=i+1}^{k'} W^{d-d}(x'_{ni}, x'_{nj}, y'_{ni} - y'_{nj}) + \sum_{i=1}^{n'}\sum_{j=1}^{k'} W^{d-d}(x'_{ei}, x'_{nj}, y'_{ei} - y'_{nj}) \\ & + \left(n - n' + k - k'\right) W_{step}, \end{aligned} \tag{3}$$

where W^{Δ} is the proper energy of the wedge disclination at the triple junction A (Fig. 2), $W^{d}(x)$ is the proper energy of an edge dislocation located at the point with coordinates (x,y) (note that the energy of a dislocation located near the free surface is sensitive to only the distance between the dislocation and the free surface [39]), $W^{\Delta\text{-}d}(d,x,y)$ is the energy that specifies the interaction between the wedge disclination A and a dislocation located at the point (x,y), $W^{d\text{-}d}(x_i,x_j,y_i\text{-}y_j)$ is the energy of the interaction between two dislocations located at the points (x_i, y_i) and (x_j, y_j), $W_{\text{step}} = \gamma_s b$ is the energy of a free surface step, γ_s is the specific free surface energy (per unit area), n and n' are the numbers of equilibrium dislocations at the GB before and after its rotation, respectively, k and k' are the numbers of non-equilibrium dislocations at the GB before and after its rotation, respectively, x_{ei} and y_{ei} are the coordinates of equilibrium dislocations at the GB in its initial state (before the rotation) (i = 1,...,n), x'_{ei} and y'_{ei} are the coordinates of equilibrium dislocations at the GB in its final state (after the rotation) (i = 1,...,n'), x_{ni} and y_{ni} are the coordinates of non-equilibrium dislocations at the GB in its initial state (before the rotation) (i = 1,...,k), as well as x'_{ni} and y'_{ni} are the coordinates of non-

equilibrium dislocations at the GB in its final state (after the rotation) (i = 1,...,k'). The dislocations of the rotating GB are numerated from the triple junction A towards the free surface (Fig. 2). The equilibrium and non-equilibrium dislocations of the GB are numerated separately.

The work of the external shear stress is given as:

$$A = \tau b \left(\sum_{i=1}^{n} s_{ei} + \sum_{i=1}^{k} (-1)^{\left\lfloor \frac{i-1}{M} \right\rfloor} s_{ni} \right), \tag{4}$$

where s_{ei} and s_{ni} are the GB-rotation-induced displacements of the ith equilibrium and the ith non-equilibrium dislocations from their initial positions, respectively; and the symbol $\lfloor x \rfloor$ denotes the integer part of x.

The energies $W^{d}(x)$, $W^{\Delta\text{-}d}(d,x,y)$, and $W^{d\text{-}d}(x_i,x_j,y_i\text{-}y_j)$ are given by the following well-known (see, e.g., [33]) expressions:

$$W^{d} = \frac{Db^2}{2}\left(\ln\frac{|x|}{b} + 1 \right), \tag{5}$$

$$W^{\Delta-d}(d,x,y) = D\omega b\left[y\cos\alpha\left(\frac{1}{2}\ln\frac{(x+d)^2+y^2}{(x-d)^2+y^2} - \frac{2xd}{(x-d)^2+y^2} \right) - \right.$$
$$\left. \sin\alpha\left(\frac{x+d}{2}\ln\frac{(x+d)^2+y^2}{(x-d)^2+y^2} - \frac{2xd(x-d)}{(x-d)^2+y^2} \right) \right], \tag{6}$$

$$W^{d-d}(x_i,x_j,y_i-y_j) = \frac{Db_ib_j}{2}\left[\ln\frac{(x_i+d)^2+y_{ij}^2}{(x_i-d)^2+y_{ij}^2} - \right.$$
$$\left. \frac{4x_ix_j\left(\left(x_i^2-x_j^2\right)^2 + 4x_ix_jy_{ij}^2 - y_{ij}^4 + 2y_{ij}\left(\left(x_i+x_j\right)^2+y_{ij}^2\right)\left(y_{ij}\cos 2\alpha - \left(x_i-x_j\right)\sin 2\alpha\right)\right)}{\left(\left(x_i-x_j\right)^2+y_{ij}^2\right)\left(\left(x_i-x_j\right)^2+y_{ij}^2\right)^2} \right], \tag{7}$$

where $D = G/[2\pi(1-\nu)]$, G is the shear modulus, ν the Poisson ratio, b_i and b_j are the Burgers vector magnitudes of the interacting dislocations, and $y_{ij}=y_i-y_j$. In formulas (6) and (7), it is necessary to take into account the sign of the dislocation Burgers vector. The disclination strength ω is related to parameters, h and b, of the wall of equilibrium dislocations in their initial positions (Fig. 2b) by the following Frank formula [40]: $b = 2h\tan(\theta/2) = -2h\tan(\omega/2)$. (As it has been noted previously, non-equilibrium dislocations in their initial positions (Fig. 2b) do not influence the mean GB misorientation figuring in the Frank formula).

From geometry of the dislocations and GBs under consideration (Figs. 2b and 2c) the numbers, coordinates and displacements of the dislocations are in the following relationship with geometric characteristics (d, h, p, α, φ) of the rotating GB:

$$n = \left\lfloor (d-b)/(h\sin\alpha) \right\rfloor, \quad n' = \left\lfloor (d-b)\cos\varphi/(h\sin(\alpha+\varphi)) \right\rfloor, \tag{8}$$

$$k = \left\lfloor (d+h/2-b)/(p\sin\alpha) \right\rfloor, \quad k' = \left\lfloor (d+h/2-b)\cos\varphi/(p\sin(\alpha+\varphi)) \right\rfloor, \tag{9}$$

$$x_{ei} = -d + ih\sin\alpha, \quad y_{ei} = -ih\cos\alpha, \tag{10}$$

$$x'_{ei} = -d + ih\sin(\alpha+\varphi)/\cos\varphi, \quad y'_{ei} = -ih\cos(\alpha+\varphi)/\cos\varphi, \tag{11}$$

$$x_{ni} = -d\left[h/2 + (i-1)p\right]\sin\alpha, \quad y_{ni} = -\left[h/2 + (i-1)p\right]\cos\alpha, \tag{12}$$

$$x'_{ni} = -d + \left[h/2 + (i-1)p\right]\sin(\alpha+\varphi)/\cos\varphi, \quad y'_{ni} = -\left[h/2 + (i-1)p\right]\cos(\alpha+\varphi)/\cos\varphi, \tag{13}$$

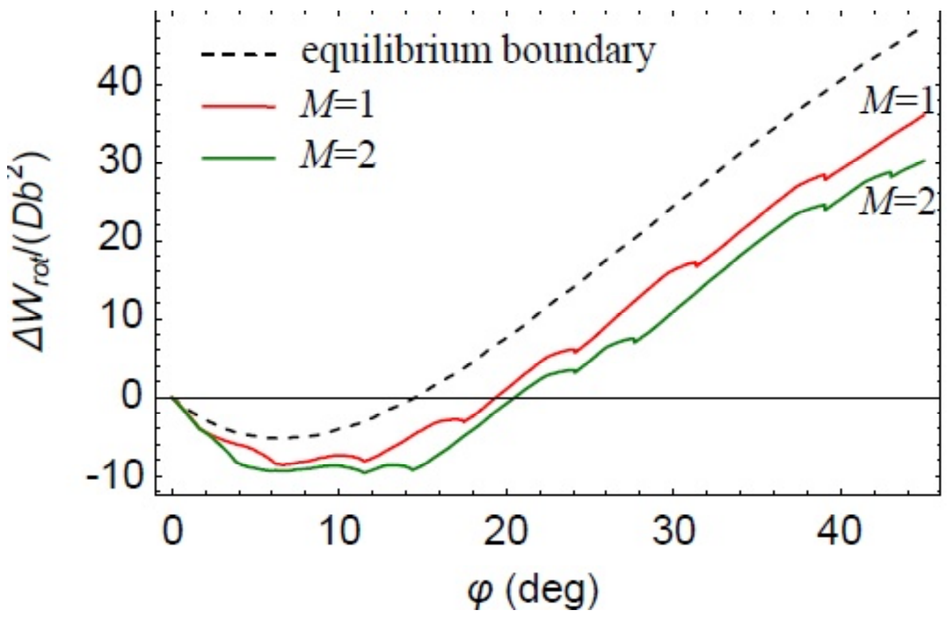

Fig. 4. (Color online) Dependences of the energy change ΔW_{rot} on rotation angle φ, for deformation-distorted grain boundaries specified by $M = 1$ and $M = 2$ as well as for the following values of other parameters: $\tau = 0.05D$, $\alpha = 45°$, $h = 5b$ ($\theta \approx 11°$), $p = h$, and $d = 100b$. Dependence $\Delta W_{rot}(\varphi)$ for non-distorted grain boundary (free from non-equilibrium dislocations) is shown as dashed curve.

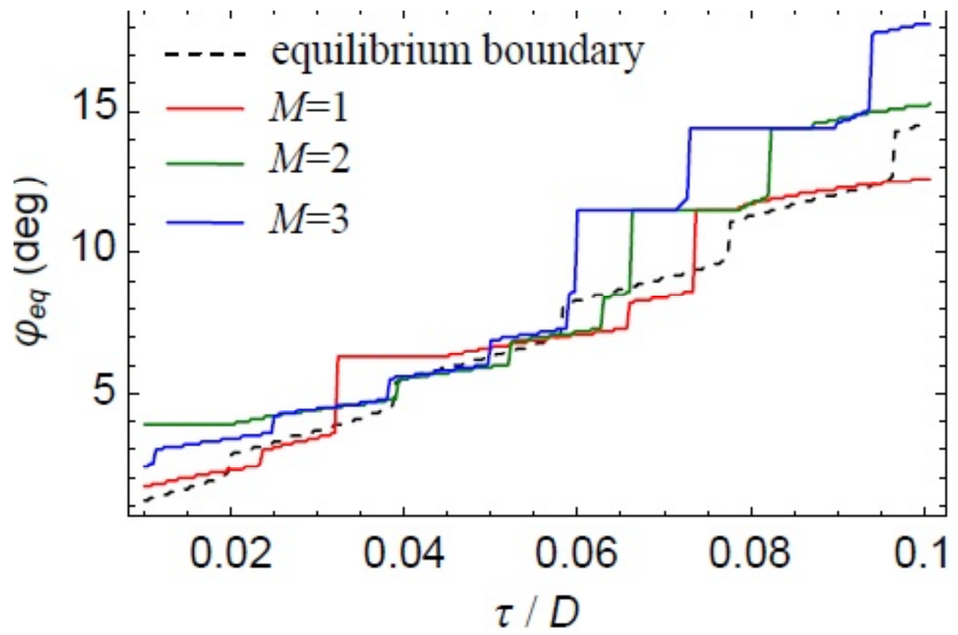

Fig. 5. (Color online) Dependences of equilibrium rotation angle φ_{eq} on the applied shear stress τ, for deformation-distorted grain boundaries specified by $M = 1$, 2, and 3 as well as for the following values of other parameters: $\alpha = 45°$, $h = 5b$ ($\theta \approx 11°$), $p = h$, and $d = 100b$. Dependence $\varphi_{eq}(\tau)$ for non-distorted grain boundary (free from non-equilibrium dislocations) is shown as dashed curve.

$$s_{ei} = \min\left(ih\tan\varphi_1, \left(\left(d-b\right)/\sin\alpha - ih\right)\tan\alpha\right), \quad (14)$$

$$s_{ni} = \min\left(\left(\left(i-1\right)p - h/2\right)\times \tan\varphi, \left(\left(d-b\right)/\sin\alpha - \left(i-1\right)p + h/2\right)\tan\alpha\right), \quad (15)$$

Here $\min(x,y)$ denotes the minimum value of x and y. In the expressions (8)–(15), the first ($i = 1$) non-equilibrium dislocation and the first ($i = 1$) equilibrium dislocation are distant by $h / 2$ and h from the triple junction A, respectively.

Thus, we found all the terms and expressions (see formulas (2)–(15)) needed for calculation of the energy change (1). With formulas (1)–(15), we calculated the energy change in the exemplary case of nickel (Ni), for the following values of its parameters [39]: $G = 73$ GPa, $\nu = 0.34$, $b = 0.25$ nm, and $\gamma_s = 2.28$ J/m^2. Fig. 4 presents typical dependences of the energy change ΔW_{rot} on the GB rotation angle φ, for $M = 1$ and 2 as well as the following values of parameters characterizing the system under examination: $\tau = 0.05D$, $\alpha = 45°$, $h = 5b$ ($\theta \approx 11°$), $p = h$, and $d = 100b$. Also, dashed curve in Fig.4 shows the dependence $\Delta W_{rot}(\varphi)$ in the previously considered [33] situation where GB is pure non-distorted, that is, does not contain any non-equilibrium dislocations.

As it follows from Fig. 4, for each of deformation-distorted and pure non-distorted GBs, the dependence $\Delta W_{rot}(\varphi)$ has at least one minimum and equilibrium rotation angle φ_{eq} corresponding to the minimum. Curves $\Delta W_{rot}(\varphi)$ for deformation-distorted GBs have pronounced jumps which correspond to events at which the dislocations enter the solid free surface. In general, the dependences $\Delta W_{rot}(\varphi)$ can have additional minima (especially in the case of $M = 2$). In this case, the system under examination has extra metastable states corresponding to the additional minima.

We now calculate and analyze the dependences of the equilibrium GB rotation angle φ_{eq} on the applied stress and basic geometric characteristics of the defect system. In doing so, in the case of a configuration having several metastable states, we will consider the state with the minimum value of φ_{eq}, that is, the (metastable) state nearest to the initial state with $\varphi = 0$. In our model, the zero temperature approximation is used, and thereby transitions between metastable states are forbidden.

Fig. 5 presents the dependences of the equilibrium rotation angle φ_{eq} on the applied shear stress τ, for $M = 1$, 2, and 3 as well as the following values of parameters: $\alpha = 45°$, $h = 5b$ ($\theta \approx 11°$), $p = h$, $d = 100b$. Also, in Fig. 5, the dependence $\varphi_{eq}(\tau)$ (dashed curve) is shown which corresponds to the case of non-distorted GB (free from non-equilibrium dislocations). Generally speaking, the dependences $\varphi_{eq}(\tau)$ for deformation-distorted GBs are similar to typical dependences $\varphi_{eq}(\tau)$ for non-distorted GB; see [33] and dashed curve in Fig. 5. At the same time, there is the specific feature inherent to the dependences $\varphi_{eq}(\tau)$ for deformation-distorted GBs. As to details, these dependences have pronounced jumps related to events of entering non-equilibrium dislocations on the free surface where the dislocations

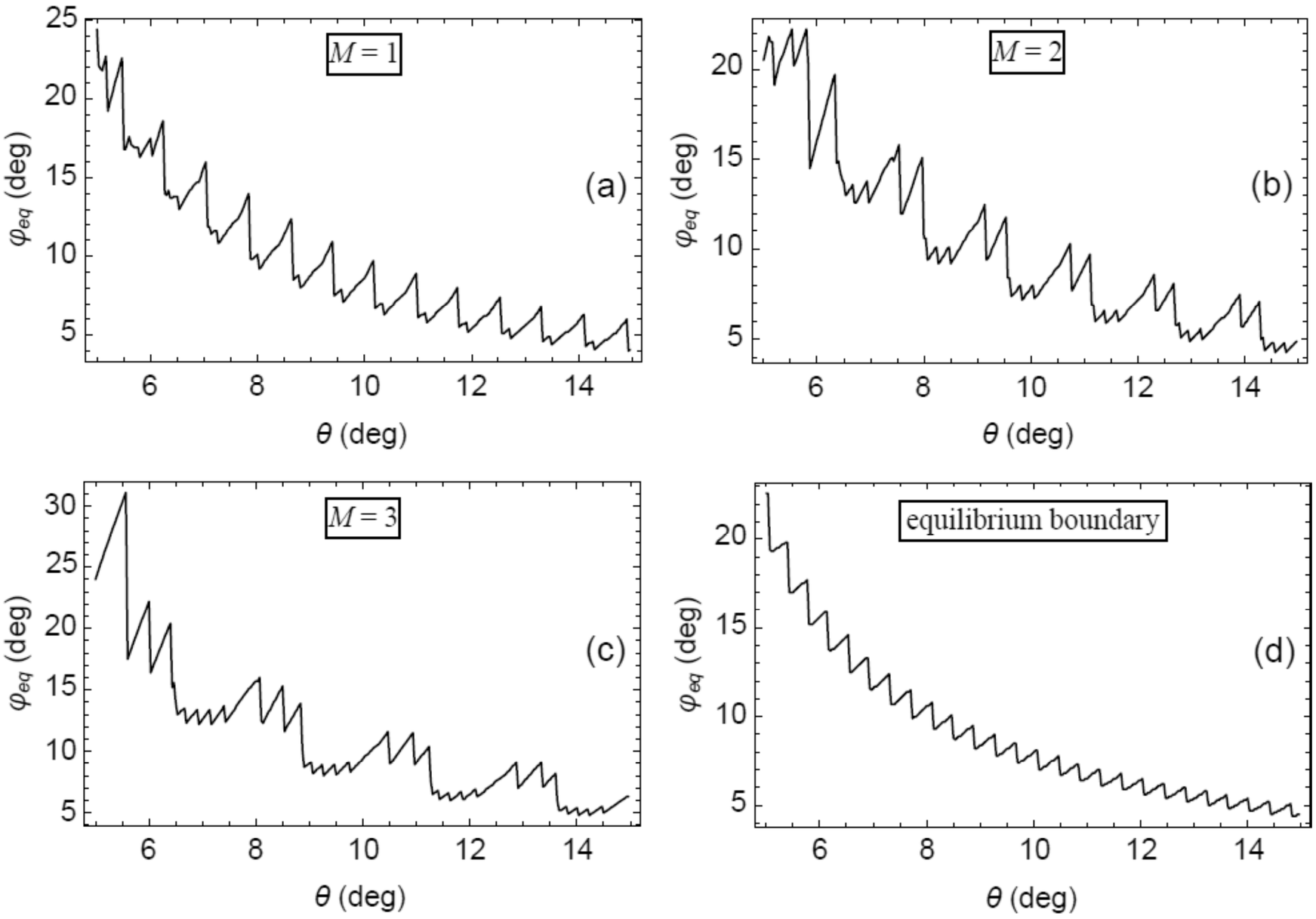

Fig. 6. Dependences of equilibrium rotation angle φ_{eq} on tilt misorientation angle θ, for deformation-distorted grain boundaries specified by (a) $M = 1$; (b) $M = 2$; and (c) $M = 3$; as well as for (d) non-distorted grain boundary (free from non-equilibrium dislocations). Other parameters of the system are taken as: $\tau = 0.05D$, $\alpha = 45°$, $p = h$, and $d = 100b$.

disappear and generate free surface steps; see Fig. 2c.

Note that when such a non-equilibrium dislocation disappears at the solid free surface, the balance between the numbers of non-equilibrium dislocations with Burgers vectors **b** and **–b** at the rotating GB is violated. That is, these numbers become different, and thereby the non-equilibrium dislocations start contributing to the tilt misorientation of the rotating GB. In the situation where the tilt misorientation decreases due to violation in the balance between the numbers of the non-equilibrium dislocations, the GB rotation is enhanced. In particular, for certain ranges of values of parameters characterizing the system, the rotation angle of a deformation-distorted GB can be significantly larger (by approximately 10°) than its values corresponding to non-distorted GBs.

With formulas (1)–(15), we calculated the dependences of the equilibrium rotation angle φ_{eq} on the tilt misorientation θ of the GB in its initial state AB and the distance d between the triple junction A and the free surface; see Figs. 6 and 7, respectively. Generally speaking, the discussed dependences for deformation-distorted GBs have the same character, as with their regular counterparts: the angle φ_{eq} rapidly decreases with rising the GB misorientation θ (Fig. 6) and slowly decreases with rising the distance d (Fig. 7). At the same time, there is the specific feature of the dependences for deformation-distorted GBs: the dependences have pronounced jumps of the angle φ_{eq} at some values of θ and d (Figs. 6 and 7, respectively). These jumps characterize enhanced rotations of the GB due to events when non-equilibrium dislocations enter on the free surface.

4. NANOGRAIN FORMATION THROUGH STRESS-DRIVEN SPLITTING AND ROTATIONS OF DEFORMATION-DISTORTED GRAIN BOUNDARIES: GEOMETRIC ASPECTS

Let us consider the geometric aspects of nanograin formation occurring through stress-driven splitting and rotations of deformation-distorted GBs in nanostructured solids. Within our model, the formation of a nanograin occurs through the following transformation of dislocations belonging to the deformation-distorted GB AB under the shear stress τ. Both the equilibrium and non-equilibrium disloca-

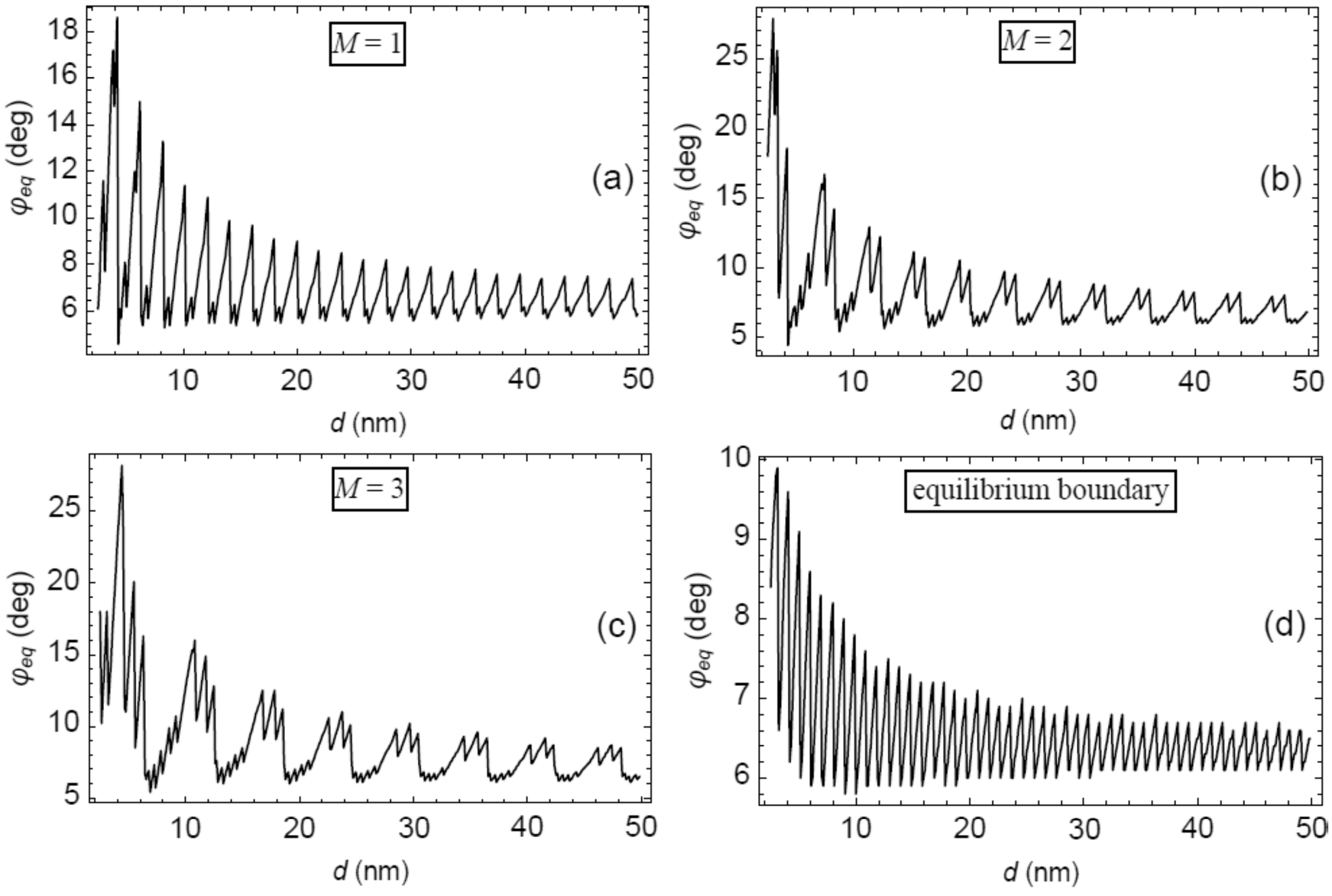

Fig. 7. Dependences of equilibrium rotation angle φ_{eq} on the parameter d (close to the length of the rotating grain boundary), for deformation-distorted grain boundaries specified by (a) $M = 1$; (b) $M = 2$; and (c) $M = 3$; as well as for (d) non-distorted grain boundary (free from non-equilibrium dislocations). Other parameters of the system are taken as: $\tau = 0.05D$, $\alpha = 45°$, $h = 5b$, and $p = h$.

tions having the same Burgers vectors **b** cooperatively move in one direction, whereas the non-equilibrium dislocations having the opposite Burgers vectors **–b** cooperatively move in the opposite direction (Fig. 2d). As a corollary, the initial GB AB splits in two GBs that rotate in opposite directions (towards their new positions AB_1 and AB_2) and form a new nanograin B_1AB_2 (Fig. 2d). This process is unique, and it comes into play due to the four effects - the *nanoscale, grain-boundary, deformation-distorted-GB-structure and free-surface effects* - operating in nanocrystalline and UFG solids containing deformation-distorted GBs. The rotation of the two GBs AB_1 and AB_2 is characterized by two rotation angles φ_1 and φ_2, respectively Fig. 2d. As it is seen in Fig. 2d, after the combined splitting and rotation process, the GB AB_1 dislocation structure is non-periodic; both the GBs AB_1 and AB_2 are asymmetric; and the sum of their tilt misorientation angles is lower than the tilt misorientation of the initial symmetric GB AB.

Note that the GB AB_2 (Fig. 2d) becomes ragged due to its rotation. That is, the distance between the end dislocation B_2 of the GB AB_2 and the free surface is larger than the GB period. In general, one can imagine the situation where new dislocations are generated at the free surface and join the GB AB_2. However, following our estimates (whose space-consuming presentation is beyond the scope of this paper), the dislocation generation at the free surface is specified by a rather high energy barrier which makes the generation process unfavorable, as compared to the rotation of the ragged GB (Fig. 2d).

5. NANOGRAIN FORMATION THROUGH STRESS-DRIVEN SPLITTING AND ROTATIONS OF DEFORMATION-DISTORTED GRAIN BOUNDARIES: ENERGY CHARACTERISTICS AND ROTATION ANGLES

Let us calculate the equilibrium rotation angles φ_1 and φ_2 (corresponding to a minimum of the energy) of the GBs AB_1 and AB_2 (Fig. 2d as functions of various parameters characterizing the system under our examination. The defect configuration shown in Fig. 2d is different from the previously considered configuration (Fig. 2c) in the only spatial arrangement of the dislocations. In these circumstances, for calculation of φ_1 and φ_2, it is convenient to exploit the approach developed in Section 3 with modifications taking into account geometry of disloca-

tion arrangement shown in Fig. 2d. In doing so, we will calculate the energy change ΔW_{split} of the defect system due to the combined splitting and rotation process (Fig. 2d). The energy change ΔW_{split} is given as:

$$\Delta W_{split} = W_1' - W_0 - A', \tag{16}$$

where W_0 and W' are the energies of the system in its initial and final states, respectively (see Figs. 2b and 2d, respectively), and A' is the work spent by the external shear stress t on the dislocation glide related to the combined GB splitting and rotation process. The energy W_0 is described by formula (2), because the initial state (Fig. 2b) is the same for the combined GB splitting and rotation process and the previously considered 'pure' GB rotation. The energy W_1' and the work A' are given by formulas (4) and (5), respectively, where the coordinates x'_{ni} and y'_{ni} as well as displacements s_{ni} of non-equilibrium dislocations in the situation illustrated in Fig. 2d are given by the following formulas (instead of formulas (13) and (15)):

$$\begin{aligned} x'_{ni} &= -d + \begin{cases} \left[\frac{h}{2} + 2(i-1)p\right]\frac{\sin(\alpha+\varphi_1)}{\cos\varphi_1}, & i \in [2NM+1, (2N+1)M] \\ \left[\frac{h}{2} + (2i-1)p\right]\frac{\sin(\alpha-\varphi_2)}{\cos\varphi_2}, & i \in [(2N+1)M+1, 2(N+1)M] \end{cases}, \\ y'_{ni} &= -\begin{cases} \left[\frac{h}{2} + 2(i-1)p\right]\frac{\cos(\alpha+\varphi_1)}{\cos\varphi_1}, & i \in [2NM+1, (2N+1)M] \\ \left[\frac{h}{2} + (2i-1)p\right]\frac{\cos(\alpha-\varphi_2)}{\cos\varphi_2}, & i \in [(2N+1)M+1, 2(N+1)M] \end{cases}, \end{aligned} \tag{17}$$

$$s_{ni} = \begin{cases} \min\left(\left(2(i-1)p + \frac{h}{2}\right)\tan\varphi_1, \left(\frac{d-b}{\sin\alpha} - 2(i-1)p - \frac{h}{2}\right)\tan\alpha\right), & i \in [2NM+1, (2N+1)M] \\ [(2i-1)p + h/2]\tan\varphi_2, & i \in [(2N+1)M+1, 2(N+1)M] \end{cases}. \tag{18}$$

In formulas (17) and (18), the upper and bottom expressions correspond to non-equilibrium dislocations having Burgers vectors **b** and –**b**, respectively. For the non-equilibrium dislocations with Burgers vectors **b**, the index i is in the range [2NM+1,(2N+1)M], where N is a non-negative integer. In the case of the non-equilibrium dislocations having Burgers vectors –**b**, the index i is in the range [(2N+1)M+1,2(N+1)M]. Other parameters (the numbers of dislocations, coordinates and displacements of the equilibrium dislocations) are given by formulas (8)–(12) and (14) where angle φ is replaced by φ_1.

Thus, we found formulas for all the terms figuring in the expression (16) for the energy change ΔW_{split}. These terms are given by formulas (2)–(12), (14), (17) and (18).

With formulas (16), (2)–(12), (14), (17) and (18), we calculated the energy change ΔW_{split} for Ni whose material parameters are given in section 3. Since the energy change ΔW_{split} represents a function of two key variables φ_1 and φ_2, it is effective to analyze its behavior in terms of the map in the coordinates φ_1 and φ_2. Fig. 8 presents the calculated map $\Delta W_{split}(\varphi_1,\varphi_2)$, for the following values of parameters: M = 1, τ = 0.05D, α = 45°, h = 5b ($\theta \approx 11°$)), p = h, and d = 100b. The energy change in the map is shown in units of Db^2. As it follows from Fig. 8, in the examined case of the combined GB splitting and rotation process, there is an equilibrium state corresponding to minimum of the energy change $\Delta W_{split}(\varphi_1,\varphi_2)$. This state is specified by equilibrium rotation angles φ_{eq1} and φ_{eq2}.

We now compare dependences of the energy change ΔW_{split} (Fig. 8) with those for ΔW_{rot} (Fig. 4). The comparison allows us to conclude that the combined GB splitting and rotation process (Fig. 2d) is more energetically favorable, as compared with "pure" GB rotation (Fig. 2c). For instance, in the case of "pure" GB rotation, the energy change ΔW_{rot} in the equilibrium state of the defect configuration has value of $\Delta W_{rot} \approx -10Db^2$ (Fig. 4), whereas the combined splitting and rotation process is characterized by value of $\Delta W_{split} \approx -25Db^2$ (Fig. 8).

After analysis of the maps $\Delta W_{split}(\varphi_1,\varphi_2)$, one can reveal the dependences of the equilibrium GB rotation angles φ_{eq1} and φ_{eq2} on various parameters characterizing the system under our examination. Below we

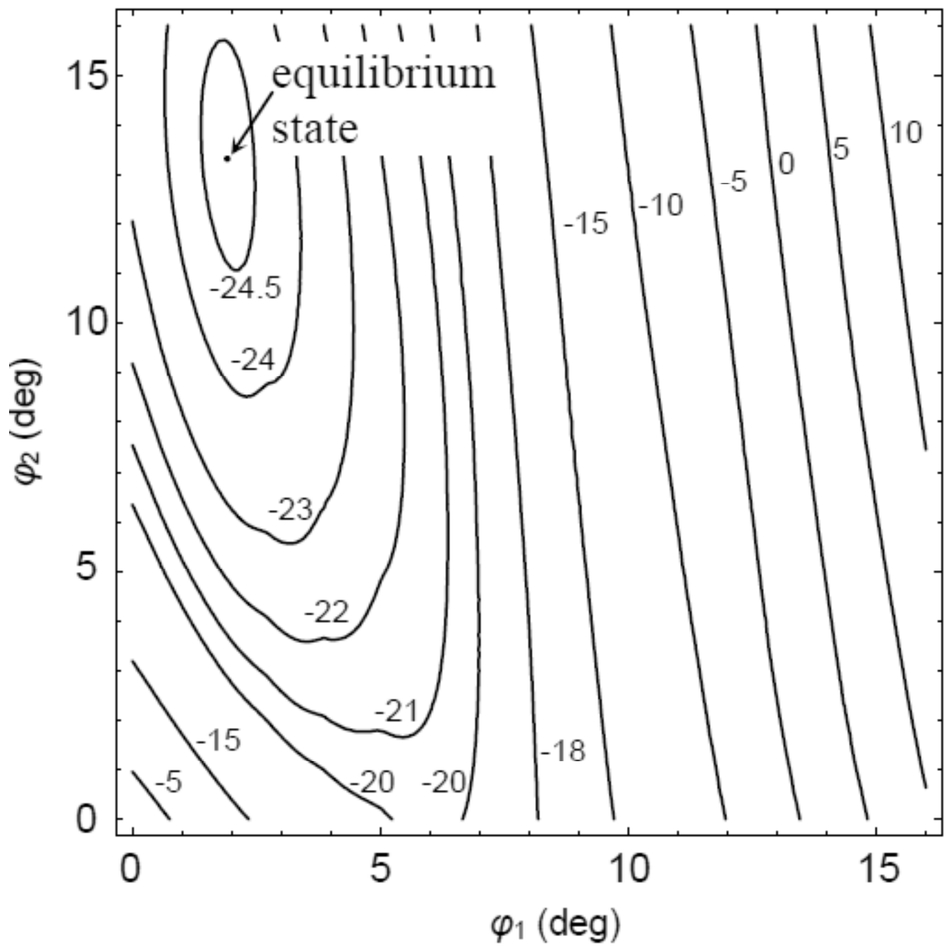

Fig. 8. Map of the energy change $\Delta W_{split}(\varphi_1,\varphi_2)$, for deformation-distorted split grain boundary specified by $M = 1$ and for the following values of other parameters: $\tau = 0.05D$, $\alpha = 45°$, $h = 5b$ ($\theta \approx 11°$), $p = h$, and $d = 100b$. The energy change is given in units of Db^2.

present these dependences (calculated from the maps $\Delta W_{split}(\varphi_1,\varphi_2)$) and compare them with the corresponding dependences presented in section 3.

So, Fig. 9 shows the dependences of φ_{eq1} and φ_{eq2} on the applied shear stress τ, for the following typical values of geometric parameters: $M = 1$, $\alpha = 45°$, $h = 5b$ ($\theta \approx 11°$), $p = h$, $d = 100b$. As it follows from Fig. 9, typical values of the equilibrium angle φ_{eq2} for rotation of the GB AB_2 are rather large (φ_{eq2}~10°–30°), and the angle φ_{eq2} rapidly grows with rising the stress τ. Also, after comparison of the dependences presented in Figs. 5 and 9, one finds that the values of φ_{eq2} are much larger than typical values (< 3°) of the equilibrium angle φ_{eq1} for rotation of the GB AB_1 (Fig. 2d) and larger than typical values (< 10°–12°; see Fig. 5) of the equilibrium angle φ_{eq} for "pure" rotation of the GB AB' (Fig. 2c). This trend is logically explained as follows. The GB AB_2 has tilt misorientation which is lower than that of the GB AB' involved in 'pure' rotation and significantly lower (by factor ~ 3, for the parameters specified above in this section) than that of the GB AB_1. As a consequence, a rotation of the GB AB_2 is enhanced as compared to those of the GB AB_1 and the GB AB'.

Note that the GB AB_2 (Fig. 2d) at some critical stress (~0.07D, for the parameters specified above in this section) exhibits unlimited rotation. This process is reflected in Fig. 9 as a dramatic (step-like) increase in the rotation angle φ_{eq2}.

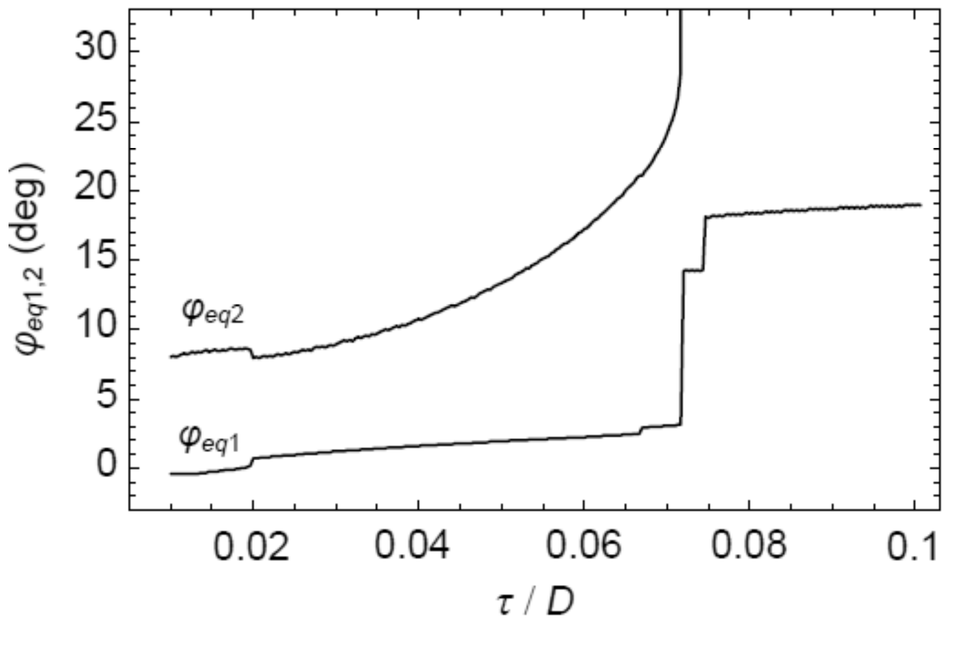

Fig. 9. Dependences of equilibrium rotation angles φ_{eq1} and φ_{eq2} on the applied shear stress τ, for deformation-distorted split grain boundary specified by the following values of parameters: $M = 1$, $\alpha = 45°$, $h = 5b$ ($\theta \approx 11°$), $p = h$, and $d = 100b$.

Fig. 10 presents the dependence of the equilibrium rotation angles φ_{eq1} and φ_{eq2} on the tilt misorientation angle θ of the initial GB AB, for the following values of parameters: $M = 1$, $\alpha = 45°$, $p = h$, $d = 100b$, and $\tau = 0.03D$. Also, Fig. 11 shows the dependence of the angles φ_{eq1} and φ_{eq2} on the distance d between the triple junction A and the solid free surface, for the following values of parameters: $M = 1$, $\alpha = 45°$, $p = h$, $h = 5b$ ($\theta \approx 11°$), and $\tau = 0.05D$. With the dependences in both these figures, one finds that the angle φ_{eq2} is significantly larger than φ_{eq1}. In doing so, the angle φ_{eq2} of the GB rotation is highly sensitive to the parameters θ and d (φ_{eq2} decreases with rising θ and/or d), whereas the angle φ_{eq1} weakly depends on θ and d. In addition, the dependences presented in Fig. 10 are indicative of unlimited rotations of the GB AB_2 in the situations where its misorientation angle becomes

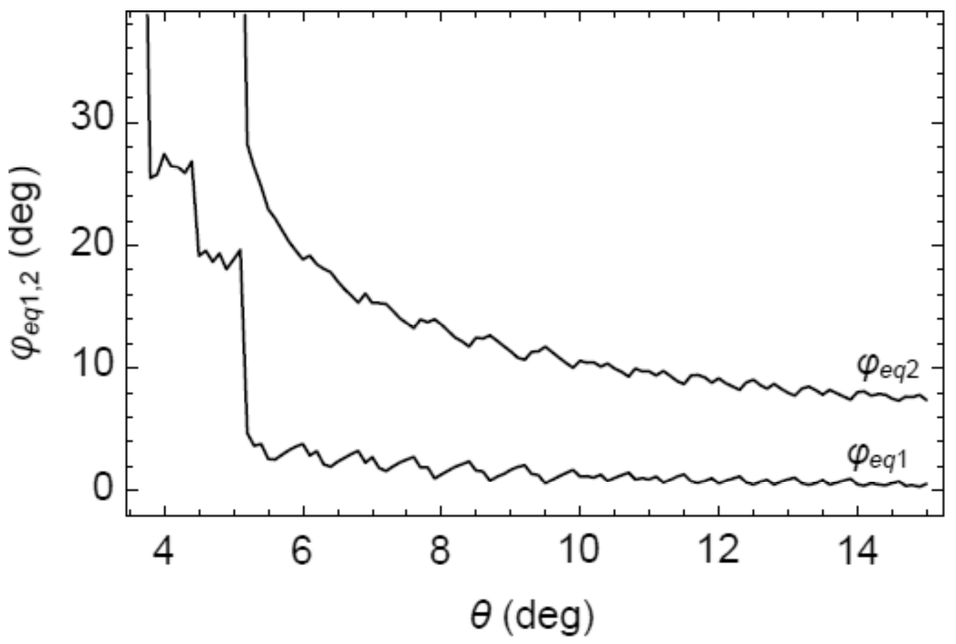

Fig. 10. Dependences of equilibrium rotation angles φ_{eq1} and φ_{eq2} on tilt misorientation θ, for deformation-distorted split grain boundary specified by the following values of parameters: $M = 1$, $\alpha = 45°$, $p = h$, $d = 100b$, and $\tau = 0.03D$.

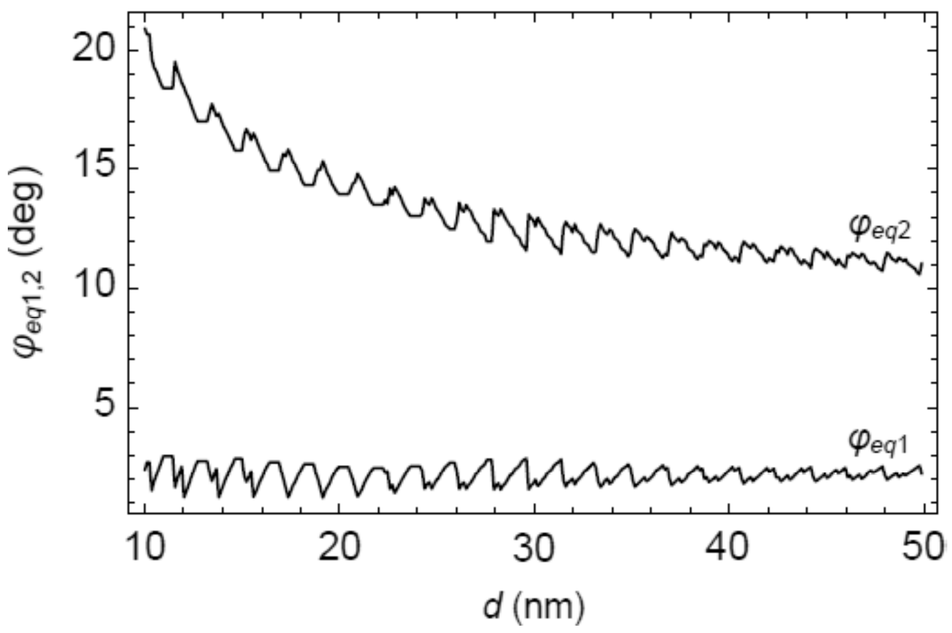

Fig. 11. Dependences of equilibrium rotation angles φ_{eq1} and φ_{eq2} on the parameter d (close to the length of the initial grain boundary AB), for deformation-distorted split grain boundary specified by the following values of parameters: $M = 1$, $\alpha = 45°$, $h = 5b$ ($\theta \approx 11°$), $p = h$, and $\tau = 0.05D$.

critically low for a given value of the applied stress. In these situations, along with the AB_2, the GB AB_1 also exhibits the unlimited rotation.

6. DISCUSSION. CONCLUDING REMARKS

Thus, a new mechanism of plastic flow – rotations of deformation-distorted GBs near free surfaces – can effectively occur in nanostructured solids (nanowires, micropillars and thin films with nanocrystalline and UFG structures as well as subsurface areas of bulk nanocrystalline and UFG materials). This conclusion results from our theoretical analysis presented in this paper and is based on representations of the model [38] describing a typical deformation-distorted low-angle GB as a dislocation wall configuration consisting of both "equilibrium" and "non-equilibrium" perfect dislocations (Fig. 3). A deformation-distorted, low-angle tilt boundary rotates through stress-driven cooperative motion of its constituent edge dislocations that carry nanoscale plastic deformation (Fig. 2c). It is theoretically demonstrated that the rotations of deformation-distorted GBs near free surfaces represent energetically favorable processes in nanocrystalline/UFG nickel in wide ranges of GB parameters. Besides, such rotations are significantly enhanced as compared to the previously examined [33] rotations of regular (non-distorted) GBs. More precisely, the equilibrium angle φ_{eq} (corresponding to minimum of the energy) for rotation of a deformation-distorted GB is typically larger by 10^o or around, as compared to its counterpart in the case of regular GBs. This enhancement is directly related to the specific effect of the deformation-distorted GB structure on nanoscale plastic flow in nanostructured solids. The rotation angle φ_{eq} for deformation-distorted GBs increases with rising the applied shear stress τ (Fig. 4), decreases with rising the GB misorientation angle θ (Fig. 5) and is weakly sensitive to the parameter d close to the GB length (Fig. 6). At the same time, the dependences of φ_{eq} on τ, θ, and d have jumps related to events of GB-rotation-induced enter of equilibrium and non-equilibrium dislocations on the free surface.

In addition to 'pure' rotation (Fig. 2c), a new phenomenon – the combined splitting and rotation of deformation-distorted GBs (Fig. 2d) - can occur and result in formation of nanoscale grains in nanostructured solids. More precisely, within our model, the initial GB AB splits in two GBs that rotate in opposite directions (towards their new positions AB_1 and AB_2) and form a new nanoscale grain B_1AB_2 (Fig. 2d). The process in question is unique, and it comes into play due to the four effects cooperatively operating in nanostructured solids containing deformation-distorted GBs. These are the *nanoscale, grain-boundary, deformation-distorted-GB-structure and free-surface effects*.

As it has been demonstrated in our examination, the nanoscale grain formation through the combined splitting and rotation of deformation-distorted GBs (Fig. 2d) is more energetically favored than the 'pure' rotation of deformation-distorted GBs (Fig. 2c). For instance, the characteristic energy profit which drives the "pure" GB rotation is by 2-3 times lower than that for the combined splitting and rotation process. Also, typical values (~10°–30°; see Fig. 9) of the equilibrium angle φ_{eq2} for rotation of the GB AB_2 resulted from the splitting process (Fig. 2d) are larger than those (< 10°–12°; see Fig. 5) of the equilibrium angle φ_{eq} for "pure" rotation of the GB AB' (Fig. 2c).

The suggested representations on GB rotation as a special deformation mode in solids are well consistent with the experimental observation [30] of GB rotations in deformed nanocrystalline Ni-4.4%W alloy nanopillars having grain size of around 60 nm. Along with GB rotation, GB migration and twinning were experimentally observed [30] in the nanocrystalline nanopillars which show smaller is softer trend. In the context of our theoretical approach presented in this paper, these experimental data are interpreted, first of all, as a manifestation of the two free-surface effects which are (i) allowance for GB parts to disappear at the free surface when it is geometrically needed, and (ii) the free-surface screening of the stress fields of defect configurations produced by GB rotation, GB migration and twinning.

Many deformation-distorted GBs are expected to exist in UFG micropillars fabricated from SPD-produced disks of Al–30%Zn alloys [31]. In the experiment [31], it was demonstrated that GB deformation mechanisms dominate in UFG micropillars where these mechanisms prevent fast plastic strain instabilities, in contrast to their coarse-grained counterpart showing fast failure due to dramatic localization of plastic flow. Our theoretical representations on enhanced rotation of deformation-distorted GBs as a GB deformation mechanism effectively operating in nanocrystalline and UFG solids - in particular, micropillars - are in agreement with the experimental data [31].

Also, the theoretical representations presented in this paper are indirectly supported by the experimental data [32] on dominant role of GB deformation mechanisms in plastic flow of nanocrystalline Au films. These films were fabricated by magnetron sputtering at highly non-equilibrium conditions, in which case the films are expected to contain a large amount of distorted GBs with extrinsic dislocations. In the experiment [32], it was demonstrated that nanocrystalline Au films are homogeneously deformed by GB deformation mechanisms (in contrast to nanocrystalline Au-Cu alloy films where GBs are effectively pinned by Cu solutes and thereby suppress GB deformation).

Note that it is very difficult to experimentally identify stress-driven rotations of GBs in nanostructured solids. The same is true for the combined splitting and rotation process (Fig. 2d). In these circumstances, we are forced to focus mainly on discussion of experimental data indirectly supporting our theoretical model. So, our theoretical representations on the combined splitting and rotation process resulting in enhanced formation of nanograins in subsurface areas of solids (Fig. 2d) is indirectly consistent with the experiments [41,42] on deformation-induced formation of the nanocrystalline structure in crystals subjected to surface mechanical attrition treatment. In the discussed experiments [41,42], nanograins with ultrasmall sizes of around 10 nm are formed within subsurface areas of metallic materials under mechanical treatment. The combined splitting and rotation process (Fig. 2d) serves a good candidate to be the micromechanism responsible for formation of such nanograins.

ACKNOWLEDGEMENTS

This work was supported, in part, (for SVB) by the Russian Ministry of Education and Science (Grant 14.B25.31.0017) and (for IAO) by the St. Petersburg State University research grant 6.37.671.2013.

REFERENCES

[1] L. Lu, M. L. Sui and K. Lu // *Science* **287** (2000) 1463.
[2] I.A. Ovid'ko // *Science* **295** (2002) 2386.
[3] M. Chen, E. Ma, K.J. Hemker, H. Sheng, Y.M. Wang and X. Cheng // *Science* **300** (2003) 1275.
[4] M.D. Uchic, D.M. Dimiduk, J.N. Florando and W.D. Nix // *Science* **305** (2004) 986.
[5] J.R. Greer and W.D. Nix // *Phys. Rev. B* **73** (2006) 245410.
[6] E. Rabkin and D.J. Srolovitz // *Nano Lett.* **7** (2007) 101.
[7] X.L. Wu and Y.T. Zhu // *Phys. Rev. Lett.* **101** (2008) 025503.
[8] X.L. Wu, Y.T. Zhu, Y.G. Wei and Q. Wei // *Phys. Rev. Lett.* **103** (2009) 205504.
[9] S.V. Bobylev and I.A. Ovid'ko // *Phys. Rev. Lett.* 103 (2009) 135501; *Phys. Rev. B* **84** (2011) 054111.
[10] Q. Yu, Z.-W. Shan, J. Li, X. Huang, L. Xiao, J. Sun and E. Ma // *Nature* **463** (2010) 335.
[11] S.V. Bobylev, N.F. Morozov and I.A. Ovid'ko // *Phys. Rev. Lett.* **105** (2010) 055504; *Phys. Rev. B* 84 (2011) 094103.
[12] Y.M. Wang, R.T. Ott, A.V. Hamza, M.F. Besser, J. Almer and M.J. Kramer // *Phys. Rev. Lett.* **105** (2010) 215502.
[13] F. Sansoz and K.D. Stevenson // *Phys. Rev. B* **83** (2011) 224101.
[14] S. Ni, Y.B. Wang, X.Z. Liao, H.Q. Li, R.B. Figueiredo, S.P. Ringer, T.G. Langdon and Y.T. Zhu // *Phys. Rev. B* **84** (2011) 235401.
[15] T. Shimokawa, M. Tanaka, K. Kinoshita and K. Higashida // *Phys. Rev. B* **83** (2011) 214113.
[16] I.A. Ovid'ko // *Appl. Phys. Lett.* **99** (2011) 0619071.
[17] J.Y. Zhang, P. Zhang, R.H. Wang, G. Liu, G.J. Zhang and J. Sun // *Phys. Rev. B* **86** (2012) 064110.
[18] Y. Zhu, Q. Qin, F. Xu, F. Fan, Y. Ding, T. Zhang, B.J. Wiley and Z.L. Wang // *Phys. Rev. B* **85** (2012) 045443.
[19] A.J. Lee, M. Kim, C. Lena and J.R. Chelikowsky // *Phys. Rev. B* **86** (2012) 115331.
[20] I.A. Ovid'ko // *Scr. Mater.* **66** (2012) 402.
[21] I.A. Ovid'ko and E.C. Aifantis // *Rev. Adv. Mater. Sci*. **35** (2013) 1.

[22] S.V. Bobylev and I.A. Ovid'ko // *Rev. Adv. Mater. Sci*. **35** (2013) 25.
[23] I.A. Ovid'ko and A.G. Sheinerman // *Rev. Adv. Mater. Sci*. **35** (2013) 48.
[24] I.A. Ovid'ko and N.V. Skiba // *Rev. Adv. Mater. Sci*. **35** (2013) 96.
[25] G. Liu, G.J. Zhang, F. Jiang, X.D. Ding, Y.J. Sun and E. Ma // *Nature Mater.* **12** (2013) 344.
[26] N.F. Morozov, I.A. Ovid'ko and N.V. Skiba // *Rev. Adv. Mater. Sci.* **37** (2014) 29.
[27] S.V. Bobylev and I.A. Ovid'ko // *Rev. Adv. Mater. Sci.* **37** (2014) 90.
[28] K. Zhou, A.A. Nazarov and M.S. Wu // *Phys. Rev. B* **73** (2006) 045410; *Phys. Rev. Lett.* **98** (2007) 035501.
[29] M.S. Wu, K. Zhou and A.A. Nazarov // *Phys. Rev. B* **76** (2007) 134105.
[30] D. Jang and J.R. Greer // *Scr. Mater.* **64** (2011) 77.
[31] N.Q. Chinh, T. Gyori, R.Z. Valiev, P. Szommer, G. Varga, K. Havancsak and T.G. Langdon // *MRS Commun.* **2** (2012) 75.
[32] J. Lohmiller, A. Kobler, R. Spolenak and P.A. Gruber // *Appl. Phys. Lett.* **102** (2013) 241916.
[33] S.V. Bobylev and I.A. Ovid'ko // *Phys. Rev. Lett.* **109** (2012) 175501.
[34] R.Z. Valiev // *Nature. Mater. Sci.* **3** (2004) 511.
[35] R.Z. Valiev and T.G. Langdon // *Progr. Mater. Sci.* **51** (2006) 881.
[36] Y. Estrin and A. Vinogradov // *Acta Mater.* **61** (2013) 782.
[37] R.Z. Valiev, I. Sabirov, A.P. Zhilyaev and T.G. Langdon // *JOM* **64** (2012) 641134.
[38] I.A. Ovid'ko, A.G. Sheinerman and R.Z. Valiev // *Scr. Mater.* **76** (2014) 45.
[39] J.P. Hirth and J. Lothe, *Theory of Dislocations* (Wiley, New York, 1982).
[40] A.E. Romanov and V.I. Vladimirov, In: *Dislocations in Solids*, vol. 9, ed. by F.R.N. Nabarro (North-Holland, Amsterdam, 1992), pp. 191–302.
[41] H.W. Zhang, Z.K. Hei, G. Liu, J. Lu and K. Lu // *Acta Mater.* **51** (2003) 1871.
[42] N.R. Tao, J. Lu and K. Lu // *Mater. Sci. Forum* **579** (2008) 91.